Lab on a Chip

Dynamic Article Links ►

Cite this: DOI: 10.1039/c0xx00000x

www.rsc.org/xxxxxx

ARTICLE TYPE

Flow enhanced non-linear magnetophoretic separation of beads based on magnetic susceptibility

Peng Li,[a] Devrim Kilinc,[a] Ying-Fen Ran,[a] and Gil U Lee*[a]

Received (in XXX, XXX) Xth XXXXXXXXX 20XX, Accepted Xth XXXXXXXXX 20XX

DOI: 10.1039/b000000x

Magnetic separation provides a rapid and efficient means of isolating biomaterials from complex mixtures based on their adsorption on superparamagnetic (SPM) beads. Flow enhanced non-linear magnetophoresis (FNLM) is a high-resolution mode of separation in which hydrodynamic and magnetic fields are controlled with micron resolution to isolate SPM beads with specific physical properties. In this article we demonstrate that a change in the critical frequency of FNLM can be used to identify beads with magnetic susceptibilities between 0.01 and 1.0 with a sensitivity of 0.01 Hz^{-1}. We derived an analytical expression for the critical frequency that explicitly incorporates the magnetic and non-magnetic composition of a complex to be separated. This expression was then applied to two cases involving the detection and separation of biological targets. This study defines the operating principles of FNLM and highlights the potential for using this technique for multiplexing diagnostic assays and isolating rare cell types.

Introduction

Superparamagnetic (SPM) beads have proven to be a highly efficient materials for separating proteins, nucleic acids, viruses, and cells, due to the high surface area, and the high rate of separation and mass transfer that takes place in highly concentrated suspensions of micron size beads.[1-5] For example, antibody and glass functionalized SPM beads are now widely used for the isolation of specific cell types and nucleic acids, respectively.[6,7] High-gradient magnetophoresis (HGM) is typically used to collect the SPM beads from complex aqueous solutions, i.e., a high magnetic field and field gradients generated by a magnet are applied to the suspension to remove the SPM beads. This technique has been fully automated for high throughput applications using electromagnets. HGM has also been used to concentrate specific analytes from a sample for lab-on-chip (LOC) applications as it provides a rapid means to analyze millilitre volume samples.[8-13] LOC devices have been used to separate SPM beads of specific size from dilute solutions by using localized laminar flow and high-gradient magnetic fields. Considering the important role magnetic separation now plays in biotechnology, there is a clear need for techniques that can quickly isolate SPM beads with specific physical properties and improve the viability of rare cell types isolated with this method.

We have recently demonstrated that a micro-magnet array (MMA) can be combined with an external rotating magnetic field to simultaneously move as many as 10^5 SPM beads in a specific direction at a defined velocity, as shown in Figure 1A.[14] The beads are trapped in the strong localized magnetic field surrounding the micro-magnets, as predicted by the finite element modelling (FEM) results shown in Figure 1B. Moreover, the beads can be moved across the MMAs by applying a rotating external magnetic field. Counter-clockwise rotation of the external magnetic field in the *xz*-plane, as shown in a series of images in Figure 1A, resulted in the movement of the SPM beads in the negative *x* direction. Non-linear magnetophoretic (NLM) transport of beads has been observed as a result of the balance between the hydrodynamic and magnetic forces that the beads experience as they move across the MMAs at a particular velocity. By using a similar technique, the effective manipulation and separation of very large amount of SPM beads has also been demonstrated.[15] A SPM bead of specific size and magnetization has a critical frequency, ω_c, at which it can no longer follow the external magnetic field because the hydrodynamic drag force on the beads increases with its velocity. The critical frequency is found to be related to the physical dimensions of the beads

$$\omega_c = \frac{\chi \mu_o \sigma_o H_{ex}}{18\eta}(2\pi\beta)^2 \exp(-2\pi\beta) \quad , \quad [1]$$

where χ is magnetic bead susceptibility, μ_o is the permeability of free space, σ_o is an experimentally determined parameter representing the effective magnetic moment of the micro-magnets, H_{ext} is the external electromagnet field strength, η is fluid viscosity, and β is the ratio of the bead radius to the distance between adjacent micro-magnets. The predicted variation in ω_c with the diameter of an SPM bead of uniform magnetization is presented in Figure 1C. The strong dependence of ω_c on β can be used to separate SPM beads of different sizes, i.e., SPM beads with a $\omega_c > \omega$ will move on the MMA while beads that have a $\omega_c < \omega$ will slow down and become immobilized at the immobilization frequency, ω_i. An analytical solution for ω_i has not been derived, but it is clear that this frequency cannot determined from simple NLM transport behavior.[16] To achieve high-resolution FNLM, the range of frequencies at which different types of beads become immobilized, i.e., $\omega_c < \omega < \omega_i$ should have minimal overlap.

HGM separation is limited in its capacity to separate SPM materials due to their tendency to interact with each other over relatively long distances resulting in the formation of chains.[5,17-21]

This has limited HGM to dilute solutions in which bead-bead interaction are unlikely to occur. FEM calculations of the local magnetic field on the MMAs, as shown in Figure 1B, revealed that the SPM beads produce little change in the local magnetic field and thus the SPM beads do not interact with each other to form chains. NLM represents a significant advance in magnetic separation because it is capable of high-resolution separation of magnetic materials based on their physical properties and it permits working with high bead densities.

We have recently demonstrated that FNLM can be achieved by applying laminar flow over the MMAs[17]. In this article, we demonstrate that FNLM can be used to separate SPM beads with high-resolution based on their magnetic susceptibility. We first describe the preparation and characterization of three SPM beads that are similar in size but have significantly different magnetic properties. We characterize the NLM transport behaviour of these beads on the microscopic scale to define the resolution and practical limitations of FNLM separation. We demonstrate that FNLM can be combined with flow cytometry to rapidly screen large number of SPM beads, and we use this technique to define the separation efficiency of the system. The FNLM transport behaviour is also analyzed using FEM to determine the influence of the beads on the local magnetic fields on the MMAs. Finally, we analyse the change in critical frequency caused by the binding of SPM beads to non-magnetic materials and experimentally demonstrate that FNLM can be used to detect and separate specific biological substances..

Materials and methods

Synthesis and characterization of magnetic beads Three SPM beads were used in this study that have similar dimensions and a low (**L**), medium (**M**), and high (**H**) level of magnetic susceptibility and saturation. The **M** beads are commercially available carboxylic acid coated M270 Dynabeads (Invitrogen, Carlsbad, CA, USA) that have been used in previous FNLM studies. The **L** beads were obtained by oxidizing the **M** beads with hydrochloric acid as described in the *Supplementary Information* (S1). The diameters of the **L** and **M** beads were measured with scanning electron microscopy (Hitachi, TM1000) and found to be 2.8 μm (coefficient of variation (CV< 3%). The density of the **M** beads was given as $1.6x10^3$ kg/m^3 by the manufacturer and this value was also used for the **L** beads. The **H** beads were synthesized by using the emulsion-templated synthesis method described previously.[22] These beads had an average diameter of 3.0 μm (CV<5%) as determined by SEM and were composed of 70% by volume Fe_3O_4 magnetic nanoparticles. The density of the **H** beads was measured to be $2.6 \pm 0.5x10^3$ kg/m^3. To minimize the adhesion forces, all three types of beads were coated with carboxylic acid groups, and the surface of the FNLM chip was treated with casein (Sigma-Aldrich). The magnetic properties of the beads were measured with a superconducting quantum interference device (SQUID) magnetometer (Quantum Design, San Diego, CA, USA) at room temperature as described previously.[23] We also used magnetophoresis to characterize the magnetic properties of individual SPM beads and the experimental details of this technique are described in the *Supplementary Information* (S2).

FNLM separation device and microscope Figure 2a presents a schematic of the key elements of the FNLM system including the separator chip, programmable electromagnets, and the liquid handling system. The FNLM separator was assembled from a micro-magnet array (MMA) that was embedded in a transparent micro-fluidic chamber. Figure 2b presents a schematic of the top-view of the separator in which the grey rectangular regions represent staggered arrays of micro-magnets[24] that are divided by 200 μm wide magnet-free channels. Figure 2c presents a microscopic image of the edge of a MMA in which circular micro-magnets can be clearly identified. The micro-magnets were composed of 5.0 μm diameter and 100 nm thick cobalt discs that were deposited on a silicon substrate on 8.0 μm centre-to-centre distance.[14,17] This MMA configuration allowed the beads to be transported in the *x* direction to the edges of the micro-magnets array by a rotating external magnetic field, and separation occurred at the edge of the arrays in the *y* direction due to hydrodynamic forces. The electromagnet system was driven with an externally programmed frequency, ω, in a four phase cycle as described previously.[17] The liquid handling system was composed of two switching valves, a programmable syringe pump for dispensing carrier fluid, a programmable syringe pump for dispensing the sample, and a sample collection manifold. By switching valve 2 fractions of the effluent could be collected at specific time intervals from the separator.

The transport of the SPM beads in the FNLM device was characterized with an optical microscope with high-speed camera and image analysis software (Zeiss Axioskop 2 equipped with AxioCam HS camera and Axiovision software). Particle imaging velocimetry (PIV) was performed in the flow cell with a Flow Master micro-PIV system and DaVis imaging software (LaVision GmbH, Germany).

A BD Accuri C6 flow cytometer (BD Biosciences, UK) was used to analyze the bead mixtures in the effluent fractions collected from the FNLM device. Laser excitations at 488 and 640 nm were used to determine the forward and side scattering properties of the beads. The fluorescence signal presented in our results was obtained by using 533 nm excitation with a 30 nm band pass filter.

FNLM separation process We analyzed the FNLM separation of the **L** and **M** beads by collecting bead fractions at specific ω. The system was loaded with the carrier fluid, i.e., phosphate buffer saline Tween (PBST, composed of 15 mM phosphate buffer, 100 mM NaCl, and 0.1% Tween 20 at pH 7.0), and the separator and micro-fluidic channels were rinsed thoroughly to remove any contaminant from previous trials. The flow rate of the carrier flow was set to 100 μl/min to maintain laminar flow in the flow chamber with minimal effects of eddy currents. This flow rate was selected to ensure that the SPM beads are not displaced from the MMA due to hydrodynamic drag and yet the rapid transport of the beads along the non-magnetic channels is allowed. A sample of **L** and **M** beads in PBST was loaded onto the micro-chip at a constant flow rate of 100 μl/min and captured on the MMAs with an external magnetic field produced by the electromagnet oriented perpendicular to the plane of the MMAs. The magnetic beads were captured on the MMA in less than 1 min after they entered the flow chamber and it took approximately 7 min to dispense the 500 μl sample of beads into the flow chamber. The SPM beads were then separated and collected at a prescribed series of ω. Beads with a critical frequency higher than the applied rotation frequency were transported on the MMA until they reached the magnet-free channels. These SPM beads subsequently were transported down the magnet-free channels in *y* direction by the hydrodynamic forces until they were released from the chip. The beads with critical frequencies lower than ω were immobilized on the MMA during the separation of beads with higher critical frequencies.

Results and discussion

Properties of the magnetic beads Figure 3a presents the magnetisation curves of the three beads that were studied with NLM. No residual magnetisation, M_r, could be detected in the **L** beads and the **M** and **H** beads had relatively low *Mr* of 0.64 and 0.97 $Am^2.kg^{-1}$, respectively. The saturation magnetization, M_s, of the **L**, **M** and **H** beads was 1.8 ± 0.2, 11.2 ± 1.0, and 65.0 ± 4.5 $Am^2.kg^{-1}$, respectively. The volumetric magnetic susceptibility, χ, of the **L**, **M** and **H** beads, calculated from the slope of the magnetization curves at magnetic fields less than 1000 Oe, was 0.02, 0.17, and 1.4, respectively. These beads span the range of magnetic properties that are currently used for HGM separation for analytical and preparative applications.

SQUID measurements in Figure 3a were made with approximately 1 mg of magnetic material and thus do not provide insight into variations in the properties of individual beads. Variations in the magnetic susceptibility of the SPM beads are quite important in this study as they could limit the precision and efficiency of FNLM separation. Microscopic measurements of magnetophoretic velocity using HGM were used to precisely determine the physical properties of individual beads. Figure 3b presents the velocities of individual **L**, **M**, and **H** beads measured in a well-defined field and field gradient. The magnetophoretic velocity of the beads was proportional to their magnetic susceptibility and square of the bead radius. The significant difference in the velocities between the three types of magnetic beads is shown in Figure 3b. The average velocity of the **M** beads was 5.6 times higher than that of **L** beads. This implies that the magnetic susceptibility of **L** beads was 5.6 times lower than that of **M** beads, as the sizes of these beads were indistinguishable. The SQUID-measured χ_M was 8.5 times larger than χ_L. The difference in the bulk and single bead measurements is attributed the differences in the density of the beads. The measured CV of the magnetophoretic velocity was 19.5%, 25.8%, and 27.8% for the **L**, **M**, and **H** beads, respectively. The measured CV of the diameter of **L** and **M** beads was less than 5% while the diameter of the **H** beads varied by as much as 15%. Magnetophoretic velocity is proportional to the square of bead radius; hence the variation in the magnetic velocity of individual beads can be attributed to the non-uniformity of their size rather than their magnetic susceptibility. This observation differs from earlier measurements of the magnetic properties of commercial beads in which larger bead-to-bead magnetizations were observed.[25]

Influence of magnetic susceptibility on NLM separation The **L** and **M** beads were selected to study the influence of the magnetic properties of the beads on the NLM transport behaviour. Figure 4 presents the average speed of these beads in *x* direction on an MMA as a function of the rotation frequency of the external magnetic field, ω. Electron micrograph images of the beads (Figure 4, insets) show no significant difference in the dimensions of the **L** and **M** beads, i.e., both beads have a mean diameter of 2.8 μm with a CV of less than 5%. Three observations can be made about the FNLM transport behaviour of these SPM beads. First, at rotation frequencies less than a threshold frequency, both beads travelled at a speed that was proportional to the rotation frequency. The threshold frequency, ω_c, was 4.0 and 25.0 Hz for the **L** and **M** beads, respectively. Second, the speed of the beads started to decrease at rotation frequencies higher than ω_c. Third, all beads were immobilized at a frequency, ω_i, of 9.0 and 41.0 Hz for the **L** and **M** beads, respectively. The differences in the NLM transport behaviour of the beads are attributed to differences in their magnetic properties.

Theoretical analysis of the forces acting on the beads in a simple one-dimensional travelling magnetic field have produced the analytical solution for NLM transport presented in Equation 1. The NLM transport equation indicates that ω_c is proportional to the magnetic susceptibility of the beads and the magnetisation of the micro-magnets, but is a nonlinear function of the physical dimensions of the beads and micro-magnets. The critical frequency of the **M** beads was measured to be more than six times larger than that of the **L** bead. This implies that the magnetic susceptibility of the **M** beads should be more than six times higher than **L** beads, which was in quantitative agreement with the measurement of the magnetization of individual **M** and **L** beads. These results confirm the validity of the simplified one-dimensional model of NLM transport and provide us with a basis for defining the performance of the separator.

Demonstration of FNLM separation based on magnetic susceptibility The difference in the NLM transport properties of the **L** and **M** beads made it possible to separate the beads in sequential steps in which the beads were first captured on the micro-magnet array and then ω was decreased in predefined steps. Mixtures of the **L** and **M** beads were separated by applying ω = 15.0 Hz to the FNLM MMA. At this frequency, the **M** beads were separated from the MMAs by laminar flow as ω was higher than the **L** bead's ω_i but lower than **M** bead's ω_c. After all the **M** beads were removed from the chip, ω was decreased to 2.0 Hz, which was lower than the critical frequency of the **L** beads, releasing the remaining L beads from the MMAs.

Figures 5a and 5b present the fluorescence-forward scattering intensity histogram and fluorescence scattering intensity histogram, respectively, of **L** and **M** beads as measured with a flow cytometer. The results presented in Figure 5a clearly demonstrate that the **L** beads produced a higher fluorescence scattering intensity and a smaller forward scattering intensity than the **M** beads. We attribute the difference in the optical signals to the oxidation of Fe_2O_3 and Fe_3O_4 nanoparticlesand a decrease in the number of iron oxide nanoparticles in the **L** beads. As seen in Figure 5b the distinct optical signature of the **L** and **M** beads made it possible to rapidly count 10^6 beads collected from the FNLM using the flow cytometer. This allowed us to quickly determine the efficiency of separation of the FNLM system under various operating conditions.

Figures 5c and 5d present the fluorescence-forward scattering and fluorescence histograms, respectively, for a three-step FNLM separation of a mixture of **M** and **L** beads. The initial 500 μl sample was composed of $5.37x10^6$ **M** and $1.02x10^7$ **L** beads. FNLM separation at 15.0 Hz resulted in the collection of $3.45x10^6$ **M** and $2.17x10^6$ **L** beads in a 1500 μl elution fraction. This initial separation resulted in an increase in the ratio of **M** to **L** beads from 0.53:1 in the initial sample to 1.59:1 in the eluted sample. Enrichment of **M** beads took place in the first FNLM separation step but a significant number of **L** beads were also collected in this fraction. We attribute this to the early displacement of the **L** beads from the micro-magnets due to their relatively low magnetic susceptibility and the weaker holding force on the micro-magnets. FNLM separation at 2.0 Hz resulted in the collection of $0.63x10^6$ **M** and $4.06x10^6$ **L** beads in a 1500 μl elution fraction. This second FNLM separation step decreased the ratio of **M** to **L** beads to 0.16:1. The residual **M** beads in the second FNLM fraction were attributed to non-ideal fluidic handling of the beads. Analysis of the overall results indicates that approximately 24% and 39% of the **M** and **L** beads were lost during separation, respectively. The majority of these beads were immobilized in the LOC device to due to nonspecific bead-surface adhesion.

These results can be used to define the separation efficiency of the FNLM process. To quantitatively analyse the FNLM performance we defined the separation efficiency of the **M** beads (SE_m) and **L** beads (SE_l) to be

$$\left.\begin{aligned} SE_m &= \frac{n_{m15}}{N_m}P_m + (1-\frac{n_{l15}}{N_l})P_l \\ SE_l &= \frac{n_{l2}}{N_l}P_l + (1-\frac{n_{m2}}{N_m})P_m \end{aligned}\right\}, \quad [2]$$

where n_{m15} and n_{m2} are the number of M beads collected at separation frequency 15.0 Hz and 2.0 Hz, respectively; N_m and N_l are the number **M** beads and **L** beads in initial mixture, respectively; and P_m and P_l are the percentage of **M** beads and **L** beads in initial mixture, respectively. This definition of separation efficiency characterized the overall performance of the system including the efficiency of capture of the desired bead. The first terms in the *SE* equations defines efficiency of isolation of the bead of desired susceptibility, while the second term defines the contribution of the undesirable beads. This definition of efficiency also takes into account the loss of any beads that takes place during separation. The calculated SE_m and SE_l from the flow cytometry measurements were 73.8% and 56.4%, respectively.

The FNLM separation process was characterized using an optical microscope, which allowed us to image the NLM separation process in specific regions of the separation chip, as shown in Figure 6a. It was clear from these microscopic studies that the SPM bead transport on the MMA was highly uniform in a particular region, which suggested the overall performance of the FNLM separation was influenced by factors other than NLM transport. Loss of the separation efficiency appears to be associated with a few factors in the FNLM system. First, the SPM beads were introduced into the separator and captured by a combination of MMA and external magnetic fields before FNLM separation started. The capturing efficiency of the **M** and **L** beads in this step was measured to be 89% and 80%, respectively. As previously noted, some beads were displaced from the FNLM chip once the high magnetic field that was used to capture the beads on the MMAs was released. These beads were collected in the 15.0 Hz elution volume resulting in a decrease in SE_m. We attribute the early release of these beads to the relatively low magnetization of the **L** beads and non-uniformity of the laminar flow field across the FNLM chip. Microscopic analysis revealed that a significant number of beads were collected in regions of the separation chamber with low hydrodynamic flow velocities resulting in the uncontrolled mixing of the separation fractions. It was also observed that a significant fraction of beads captured on the MMAs did not move even after ω was decreased to 2.0 Hz. We attribute this behaviour to adhesive interactions of the bead with the surface of the separator. Acid treatment of the **L** beads appears to have made them more prone to adhesive interactions.

Optimization of the properties of the SPM beads for efficient separation Figure 1C presents the relationship between ω_c and the diameter of a bead calculated using the one-dimensional NLM equation. It is clear from this relationship that the magnitude of ω_c increases with the diameter of the magnetic bead until it reaches about five times the distance between adjacent micro-magnets, after which it decreases as the diameter of the bead increases. Large values of ω_c are desirable for FNLM separation as they lead to higher separation speeds and the capacity to use a wider range of separation frequencies. Our MMAs currently have a 2.0 ± 0.2 μm gap between micro-magnets and this dimension is unlikely to decrease below 0.5 ± 0.2 μm unless the fabrication costs are significantly increased. The diameters of the SPM beads we have studied to date are smaller than 3 μm, but SPM beads as large as 5.0 μm can be used in the current MMA design. SPM beads smaller than 0.5 μm in diameter are not recommended for use in FLNM due to their low ω_c and low separation speed. Another disadvantage of using smaller beads is the difficulty of capturing them on the MMA.[5]

The performance of the FNLM separation was strongly influenced by the magnetic properties of the beads and micro-magnets. From the one-dimensional NLM equation it is clear that ω_c increases with increasing χ, σ_o, and H_{ext}. This suggests that the use of SPM beads with higher susceptibilities will increase the speed and resolution of the FNLM separation. The one-dimensional NLM equation can also be used to predict the minimum magnetic susceptibility that can practically be used in the FNLM. A lower limit of 1 Hz was set to ω_c to meet the target separation duration of several minutes. A 1.0 Hz critical frequency for a 2.8 μm beads corresponds to a χ of 0.007 based on the linear relationship between the critical frequency and magnetic susceptibility at low ω. These results suggest that magnetic beads with susceptibilities higher than 0.01 and a diameter between 0.5 and 5 μm are optimal for FNLM separation using our current generation of MMAs. Increasing the magnetic moment of the micro-magnets and magnitude of the external magnetic field will also improve FNLM performance.

Magnetic bead chain formation It has previously been observed that SPM beads form chains in homogeneous magnetic fields as a result of dipole-dipole interactions.[5] This has made it difficult to apply HGM to high-resolution magnetic separation as chains of varying numbers of beads have significantly different magnetic velocities. An important feature of FNLM separation is that the SPM beads are exposed to an external magnetic field in the presence of a MMA. For example, the micrographs in Figure 1a show dispersed **M** beads on a MMA as the external magnetic field is rotated through 360°. Figure 1b presents the magnetic potential energy distribution calculated with FEM for three **M** beads on four micro-magnets as a function of ω. It is clear from these results that potential energy barriers, i.e., the regions of blue colour, form between the SPM beads and prevent them from forming chains. As the external magnetic field is rotated in the *xz*-plane of the chip the potential minima travel across the micro-magnets resulting in the movement of the SPM beads from right to left. Due to the comparable sizes of the potential well and SPM beads at each phase of the external field, individual beads are confined in the potential energy minima and do not strongly interact with adjacent beads.

Figure 6 presents optical micrographs of the **M** and **H** SPM beads on micro-magnet arrays in the presence of an external magnetic field. Large aggregates of **H** beads can be seen on the micro-magnet arrays in Figure 6B suggesting that the properties of these SPM beads can lead to the formation of chains. FEM was used to determine the magnetic potential energy landscape distribution on the micro-magnets array for different SPM bead susceptibilities to understand how the bead susceptibility affects the potential energy distribution. Figure 7 presents the results of the FEM calculations for closely packed SPM beads with uniform susceptibilities ranging from 0 to 2.5. The potential energy distribution of the **M** beads is presented in Figure 7b. In this case, it is clear that the magnetic energy distribution was dominated by the micro-magnets and the beads did not form chains. At the susceptibility of the **H** beads, i.e., a χ of 1.5, the potential energy

distribution was dominated by the fields produced by the SPM beads and magnetic energy minima formed at the point of contact between the beads. This is consistent with the observation that the **H** beads were attracted to each other and formed chains on the MMAs.

These results can be explained in terms of the scaling laws that define the magnetic potential energies that the bead experiences. The magnetic bead dipole moment, *m*, in an external magnetic field, *H*, produced by the MMA and the external electromagnetic field is

$$m = \frac{4}{3}\rho a^3 \mu_o \chi H \quad [3],$$

where *a* is bead radius, μ_o is the magnetic constant, and χ is the susceptibility of the bead.[26] The dipole-dipole interaction energy between two SPM beads aligned in an external magnetic field is

$$U_{mag} = \frac{|m|^2}{16\rho\mu_o a^3} \quad [4].^{27}$$

The magnetic energy between the SPM bead's dipole moment and the external magnetic field produced by the micro-magnet is

$$U_{ex} = |m| H \quad [5].$$

Clearly, the bead–bead interaction is a quadratic function of the SPM bead susceptibility, χ, while the bead–micro-magnet interaction has a linear dependence on χ.[28] At low χ, the bead–micro-magnet interaction is stronger than the bead–bead interaction. As the χ of the SPM beads exceed 1, the interaction between the beads rapidly increases and ultimately dominates the overall interaction energy. This results in the formation of bead chains which are impossible to implement in FNLM. We can define a susceptibility threshold, χ_c, at which bead chains form. At χ_c, the depth of the potential energy well between the bead and micro-magnets is equal to the potential energy at the point of contact of the bead–bead interaction. The results of FEM simulations of SPM beads with varying χ, shown in Figure 7, indicate that χ_c will be located between 1.0 and 1.5. This susceptibility range is one order of magnitude higher than the susceptibilities of commercially available SPM beads. Higher values of χ_c can in principle be achieved by producing micro-magnets with a higher magnetic moments (σ_o) and using stronger external magnetic fields (H_{ex}).

Biological separation In magnetic separation we seek to isolate specific biological substances such as biomolecules and cells from complex mixtures, based on their preferential binding to SPM beads. Formation of a complex with the biological substance will change both the magnetic susceptibility and the hydrodynamic radius of the SPM bead. In this study, we have accurately described the ω_c of an SPM bead as a function of its magnetic susceptibility, μ, and radius, *a* (Equation 1). The FNLM transport properties of a biological substance–SPM bead complex can be easily derived if we assume that only one bead reacts with the biological substance. The equation for the critical frequency of the bio-conjugated SPM bead complex is then

$$\omega_c = \frac{\chi\mu_o\sigma_o H_{ex} a}{18\eta r}(2\pi\beta)^2 \exp(-2\pi\beta) = \omega_c \frac{a}{r} \quad [6],$$

where *r* is the effective hydrodynamic radius of the complex. This relatively simple expression indicates that high-resolution FNLM separation can be achieved by applying it to biological substance–SMP bead complexes that are relatively large compared to the bare SPM beads.

To test the validity of Equation 6, we have applied it on FNLM separation experiments conducted with several biomaterials. We selected *S. cervisiae* as a model for FNLM separation of cells due to its relatively small size, i.e., diameter of 4 to 5 μm, and stability. In a previous study, we demonstrated that the binding of *S. cervisiae* to an **M** bead produced a decrease in the critical frequency from 4.5 Hz to 3.0 Hz (Fig. 4A in ref. 14). We note that the critical frequencies in this study are quite a bit higher than this study, because of the improvement in the MMAs used. The experimentally-observed decrease in the ω_c of the complex is consistent with the theoretical decrease in ω_c predicted by Equation 6, i.e., the hydrodynamic radius of the *S. cervisiae*–**M** bead complex increased approximately 50% compared to that of the bare **M** bead. This shift in ω_c was sufficient to achieve both the detection and efficient separation of the *S. cervisiae*–**M** bead complex from the bare SPM beads.

To demonstrate the limit of biological separation resolution we also coated the **M** beads with a monolayer of exosomes isolated from *in vitro* cultures of pancreatic cancer cell lines. This monolayer was created by activating the **M** beads with N-hydroxysuccinimide-1-ethyl-3-(3-dimethylaminopropyl) carbodiimide (Sigma-Aldrich) followed by incubation with an excess of exosomes. The nominal diameter of these size selected exosomes was 120 nm. Figure 4 shows that the critical and immobilization frequencies of the exosome–SPM bead complex were 23.0 Hz and 37.8 Hz, respectively. The experimentally-observed 8% decrease in ω_c was consistent with the theoretical decrease in ω_c predicted by Equation 6, i.e., the hydrodynamic radius of the exosome–**M** bead complex was about 8% larger than that of the bare **M** bead. Separation of the exosome–bead complex from bare **M** beads is difficult due to the small difference in their ω_c and ω_i. However, the 8% shift in ω_c can be clearly detected when the FNLM spectra of bare and exosome-coated **M** beads are compared (Figure 4).

Conclusions

In this article we provide a first definition of the influence of the magnetic properties of SPM beads on the efficiency of FNLM separation. SPM beads that had similar dimensions but different magnetic properties were produced and carefully characterized. The use of the FNLM separator along with a flow cytometer provided a rapid means for the identification of large numbers SPM beads of specific magnetization and size. The current FNLM device is capable of separating SPM particles that are 0.5 to 5 micron in diameter, which is consistent with prokaryotic and eukaryotic cell dimensions, and with a magnetic susceptibility between 0.02 and 1.0. At higher magnetic susceptibilities, the beads formed chains on the MMAs. FNLM was used to separate SPM beads with susceptibilities between 0.02 and 0.17 based solely on their magnetic properties with an overall separation efficiency of 56% and 74%, respectively. The resolution of the FNLM separator was approximately 0.01 susceptibility units per Hertz. Microscopic analysis of the system revealed that the NLM process was highly efficient, and efficiency losses stemmed from the low holding forces acting on low-magnetization SPM beads, non-uniformity of the flow, entrapment of the beads in dead volumes in the fluidic setup, and the adhesion of SPM beads to the internal surfaces of the device. We are confident that each of these factors can be addressed through the optimization of the design and micro-fabrication of the FNLM system. The critical frequencies of complexes consisting of non-magnetic biological substances and SPM beads have been theoretically derived. This

derivation allows us to predict the FNLM detection and separation performance for biological targets. Based on these results, the FNLM system was used to separate and detect *S. cervisiae*- and exosome-coated **M** beads. This technique promises to be highly useful for the identification of multiple biomarkers and isolation of specific cell types based on their reaction with antibody-functionalized SPM beads of defined magnetisation and size.

Acknowledgements

This work was supported by the Science Foundation of Ireland (08/RP1/B1376 and 08/IN1/B2072), Irish Research Council (EMPOWER) for PL, and Marie Curie Intra-European Fellowship for DK. We thank Amanda McCann, Mark Platt, James O'Mahony, Alfonso Blanco, and Ian Reid for their helpful advice and supply of materials.

Notes and references

[a] *Centre for Nanomedicine, School of Chemistry and Chemical Biology, University College Dublin, Belfiled, Dublin 4, Ireland.*

† Electronic Supplementary Information (ESI) available: [details of any supplementary information available should be included here]. See DOI: 10.1039/b000000x/

Supplementary Information

S1. Synthesis of low magnetiization beads. A 250 µl volume of neat M270 Dynabeads beads was placed in a centrifuge tube and washed twice with deionized water before resuspending them in 500 µl DI water. A 500 µl volume of concentrated hydrochloric acid was added to the beads and suspension was placed on a rotating wheel for 3 hours, after which the beads had changed from an orange/brown to yellow colour. A black color is characteristic of Fe_3O_4 nanoparticles while Fe_2O_3 nanoparticles have a yellow/red color. The beads were collected with a permanent magnet and washed three times with DI water to stop the reaction. They were then coated with 1 ml of 5% (w/w) polyethyleneimine solution in a sodium carbonate buffer for 2 hours, followed by three DI water washes. A 1 ml volume of 5% polyacrylic acid-maleic acid solution was then added to the beads at room temperature for 2 hours, before being washed three times with DI water and then suspended in PBST.

S2. Measurement of the magnetophoretic velocity of magnetic beads. Magnetic properties of the **L**, **M**, and **H** beads were characterized by measuring the velocity of the beads under constant magnetic field [29]. This technique is based on the fact that at equilibrium, the magnetic force, F_m, applied to a bead is equal to the viscous drag force, F_h. The magnetic force acting on a bead under an external field is

$$F_m = (m \cdot \nabla)B = \frac{V \times \chi}{m_o}(B \cdot \nabla B) \ ,$$

where, m is magnetic dipole of the bead, B is external magnetic field, V is the bead volume, χ is the bead susceptibility, and μ_o is the magnetic permeability of a vacuum. The hydrodynamic force acting on a bead is

$$F_h = -6\pi\eta a v f_D \ ,$$

where η is kinematic viscosity of the fluid, a is the bead radius, v is the bead speed, and f_D is drag factor of the bead. Thus, for a known size of bead and hydrodynamic factors, the magnetic forces acting on the bead and the magnetic moment of the bead can be calculated. The magnetic susceptibility of the bead is

$$\chi \propto \frac{v}{r^2}$$

for the same magnetic field and fluidic properties. Since the **L** and **M** beads have the same diameter and are subjected to the same magnetic field and field gradients, the magnetic susceptibility is proportional to drag velocity. The average size of **H** beads was slightly larger than that of **L** and **M** beads. To determine the susceptibility differences between the H and M beads the measured velocities of were corrected by a size factor.

The magnetic field was imposed by two pairs of NdFeB magnets 12.7×12.7×6.35 mm in size with a 1 mm air gap separating the two like poles[20]. An aluminium magnet holder was attached to a micromanipulator (Eppendorf, Hamburg, Germany) to bring the magnets over the imaging field of an inverted microscope (Aviovert, Zeiss, Hertfordshire, UK) at desired distances from the beads. Magnetic beads and fluorescent microspheres (Polysciences, Warrington, PA) were mixed in a 55% (w/w) sucrose solution and a magnetic force was applied in the plane of the flow cell by bringing the magnet assembly at 3 mm distance from the imaging field. The strong optical activity of the magnetic beads made it easy to identify them with transmitted light using a 40× objective. The bead movement was recorded using an EMCCD camera (Hamamatsu, Hertfordshire, UK) at 3.3 fps and the drag velocity of beads were measured by tracking beads using the NIH ImageJ software. The relative average lateral velocity was calculated by using the position of fluorescent beads as reference.

References

1. A. Heeboll-Nielsen, S. F. L. Justesen, T. J. Hobley and O. R. T. Thomas, *Separation Science and Technology*, 2004, 39, 2891-2914.
2. S. Bucak, D. A. Jones, P. E. Laibinis and T. A. Hatton, *Biotechnol. Prog.*, 2003, 19, 477-484.
3. J. Muzard, M. Platt and G. U. Lee, *Small*, 2012, 8, 2403-2411.
4. C. Fields, J. Muzard, P. Mallee and G. U. Lee, *Food Chemistry*, 2012, 134, 1831-1838.
5. W. S. Chang, H. Shang, R. M. Perera, S. M. Lok, D. Sedlak, R. J. Kuhn and G. U. Lee, *Analyst*, 2008, 133, 233-240.
6. J. G. Treleaven, F. M. Gibson, J. Ugelstad, A. Rembaum, T. Philip, G. D. Caine and J. T. Kemshead, *Lancet*, 1984, 1, 70-73.
7. M. Uhlen, *Nature*, 1989, 340, 733-734.
8. M. A. M. Gijs, F. Lacharme and U. Lehmann, *Chemical Reviews*, 2010, 110, 1518-1563.
9. H. Ueda, K. Agatsuma, K. Kajikawa, M. Furuse, S. Fuchino and A. Ishiyama, *Ieee Transactions on Applied Superconductivity*, 2009, 19, 2157-2161.
10. H. Chen, A. D. Ebner, D. Bockenfeld, J. A. Ritter, M. D. Kaminski, X. Liu, D. Rempfer and A. J. Rosengart, *Physics in Medicine and Biology*, 2007, 52, 6053-6072.
11. K. H. Han and A. B. Frazier, *Lab Chip*, 2006, 6, 265-273.
12. N. Pamme, *Lab on a Chip*, 2006, 6, 24-38.
13. M. A. M. Gijs, *Microfluidics and Nanofluidics*, 2004, 1, 22-40.
14. B. B. Yellen, R. M. Erb, H. S. Son, R. Hewlin, H. Shang and G. U. Lee, *Lab on a Chip*, 2007, 7, 1681-1688.
15. M. Donolato, B. T. Dalslet, and M. F. Hansen, Biomicrofluidics, 2012, 6, 024110.
16. L. Gao, N. J. Gottron III, L. N. Virgin, and B. B. Yellen, *Lab on a chip*, 2010, 10, 2108-2114.
17. P. Li, A. Mahmood and G. U. Lee, *Langmuir*, 2011, 27, 6496-6503.
18. I. Petousis, E. Homburg, R. Derks and A. Dietzel, *Lab on a Chip*, 2007, 7, 1746-1751.
19. E. Climent, M. R. Maxey and G. E. Karniadakis, *Langmuir*, 2004, 20, 507-513.

20. S. L. Biswal and A. P. Gast, *Analytical Chemistry*, 2004, 76, 6448-6455.
21. R. Pastor-Satorras and J. M. Rubi, *Journal of Magnetism and Magnetic Materials*, 2000, 221, 124-131.
22. H. Shang and G. U. Lee, *Journal of the American Chemical Society*, 2007, 129, 6640-6646.
23. H. Shang, W. S. Chang, S. Kan, S. A. Majetich and G. U. Lee, *Langmuir*, 2006, 22, 2516-2522.
24. L. Johansson, K. Gunnarsson, S. Bijelovic, K. Eriksson, A. Surpi, E. Gothelid, P. Svedlindh and S. Oscarsson, *Lab on a Chip*, 2010, 10, 654-661.
25. D. R. Baselt, G. U. Lee, M. Natesan, S. W. Metzger, P. E. Sheehan and R. J. Colton, *Biosensors & Bioelectronics*, 1998, 13, 731-739.
26. S. L. Biswal and A. P. Gast, *Physical Review E*, 2004, 69, 041406.
27. Y. Nagaoka, H. Morimoto and T. Maekawa, *Physical Review E*, 2005, 71.
28. A. Fortini and M. Schmidt, *Physical Review E*, 2011, 83, 041411.
29. D. Kilinc, A. Blasiak, J. J. O'Mahony, D. M. Suter and G. U. Lee, *Biophysical J*, 2012, 103, 1120-1129.

Figures

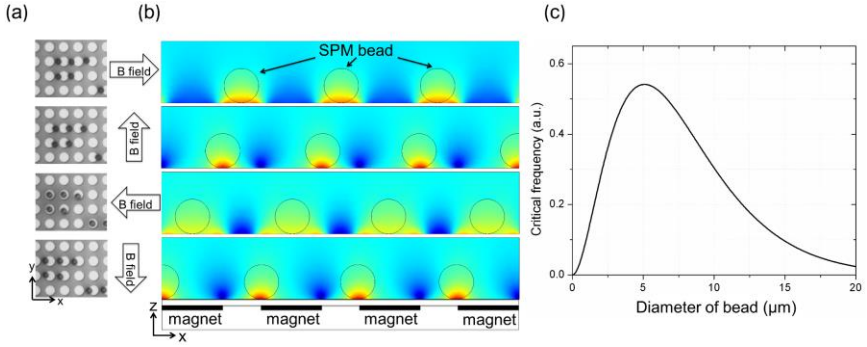

Fig. 1. Non-linear magnetophoretic transport of SPM beads on a MMA. (a) Top view optical micrographs of SPM beads on 5 μm diameter micro-magnets at four different angles of external magnetic field, i.e., θ_{xz}=0°, 90°, 180°, and 270°(top to bottom). (b) Finite element modeling of the magnetic potential energy distribution, U_{tot}, above the MMA in the presence of SPM beads with a magnetic susceptibility, χ =0.17. An external magnetic field of 60 Gauss was rotated through θ_{xz}=0°, 90°, 180°, and 270°. The micro-magnets have been drawn underneath the finite elements results to illustrate how the local and external fields combine to produce a traveling magnetic potential energy distribution. The warm colours represent the lowest potential energy and represent a point that the beads move towards. (c). Theoretical critical frequency as a function of the bead diameter (χ =0.17) for the 5 micron diameter cobalt micromagnets used in this study. The critical frequency initially increases as the bead diameter increases to approximately 5 μm, after which the critical frequency decreases.

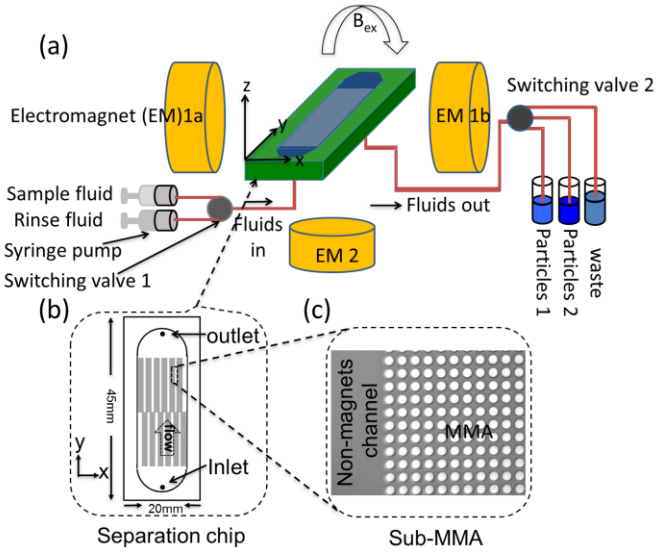

Fig.2. The flow enhanced non-linear magnetophoresis system. (a) Schematic of FNLM separator components which include a separation chip *(SC)*, a set of programmable electromagnets *(EM1 and 2)* for generating the rotating magnetic field, syringe pumps, switching valve, and fluid collection system. (b) Schematic of the separation chip consisting of staggered MMAs (grey rectangles) that were divided by non-magnets channels (white areas). During FNLM separation the SPM beads were captured on the MMA, transported in *x*-direction to the edges of the MMA, and transported downstream in the y-direction in the non-magnetic channels. (c) Optical micrograph of the edge of a MMA composed of a lattice of 5 μm circular cobalt micro-magnets (white circles) on 8 μm centres

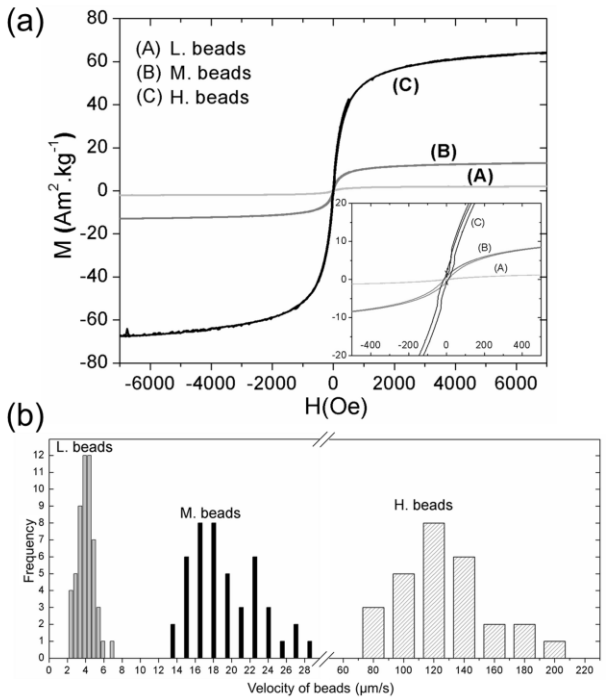

Fig. 3. Properties of the **L**, **M** and **H** SPM beads. (a) SQUID magnetometry characterization of the **L**, **M**, and **H** SPM beads at room temperature. Each of the three beads had a different saturation magnetization and magnetic susceptibility. (b) Histogram of the magnetphoretic velocity of **L**, **M**, and **H** of individual SPM beads. The velocity of the beads was proportional to the magnetic susceptibility and the square of the diameter of the beads. The velocity of at least 20 individual beads was measured.

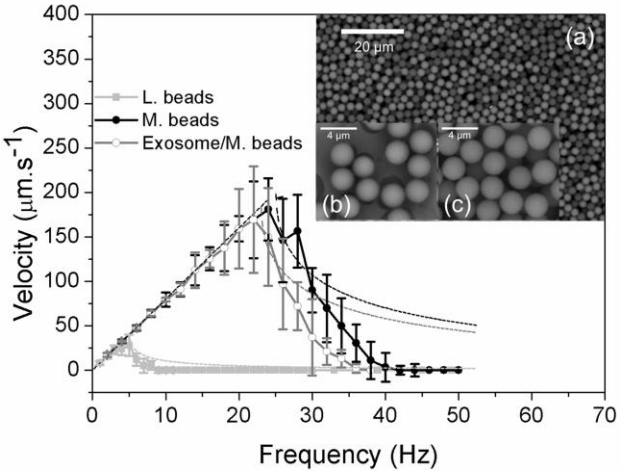

Fig. 4. Average velocity of the **L, M** beads, and exosome coated **M** beads as a function of the rotation frequency of external magnetic field. The beads speed was proportional to rotation frequency of the external magnetic field at the frequency below the critical frequency, which was 4.0Hz, 25.0 Hz, and 23.0 Hz for the **L**, **M** beads, and exosome coated **M** beads, respectively. The immobilization frequency, the frequency above which the beads were completely immobilized, was 9.0 Hz, 42.0 Hz, and 37.8 Hz for **L, M** beads, and exosome coated **M** beads, respectively. These measurements were made with at least 15 separated beads using a microscope and high-speed camera. The dotted lines in the graph are the theoretical velocities calculated by using Equation (1). (Inset) Backscattered SEM images of **L** and **M** beads. (a) Mixtures of two beads show no detectable size difference but a significant difference in backscattered signature. We attributed the higher back scattering signal of the **M** beads to a higher Fe_3O_4 nanoparticle composition. The images in the lower, left corner are higher resolution SEM images of the **M** beads (b) and the **L** beads (c).

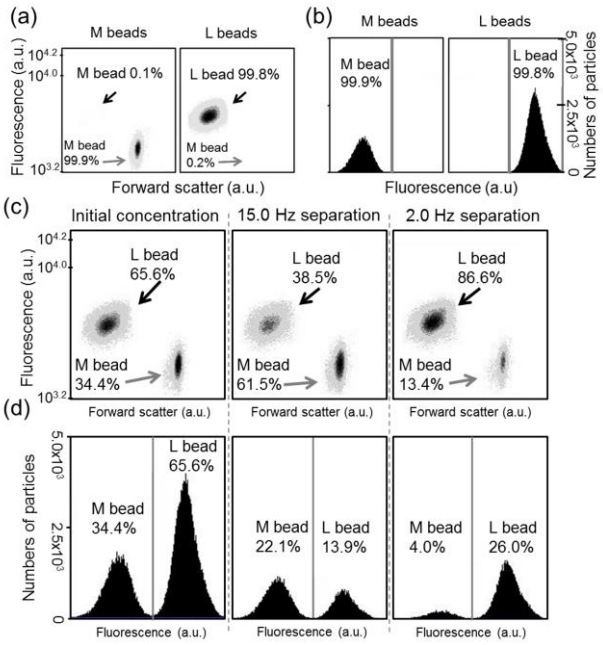

Fig. 5. Separation efficiency of the FNLM system for the **L** and **M** beads. (a) Histograph of fluorescence (side scatter signal using a 533/30 nm emission filter and 488nm and 640nm excitation) intensity as a function of forward scattered intensity for pure **M** and **L** beads. Flow cytometry can be used to quickly identify the two types beads because **L** beads have a higher fluorescence and lower forward scattered intensity. (b) Identification of the **M** and **L** beads using only the fluorescence intensity. (c) Analysis of the FNLM separation results using fluorescence and forward scattering intensity. These three graphs illustrate the change in the concentration of **M** and **L** beads in the FNLM fractions collected at an external magnetic field rotation frequency of 15 Hz and 2 Hz. (d) Analysis of the FNLM separation efficiency using fluorescence intensity only.

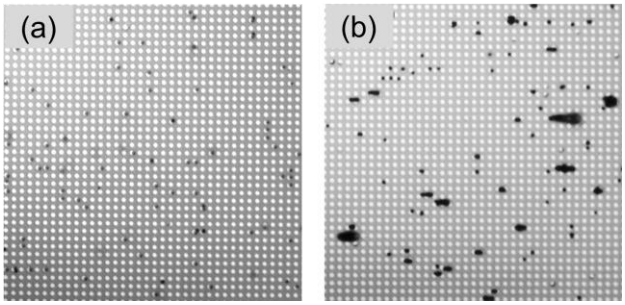

Fig. 6. Influence of SPM bead magnetic susceptibility on NLM transport behavior. (a) Optical micrograph of **M** beads (black circles) on micro-magnets (white circles). (b) Micrograph of **H** beads on a MMA as the external magnetic field rotates at 2 Hz. A large number of SPM bead form chains due to relative strong bead-bead interaction. The chains of beads rotate on the MMA but have different critical frequencies due to variations in the number of beads in each chain.

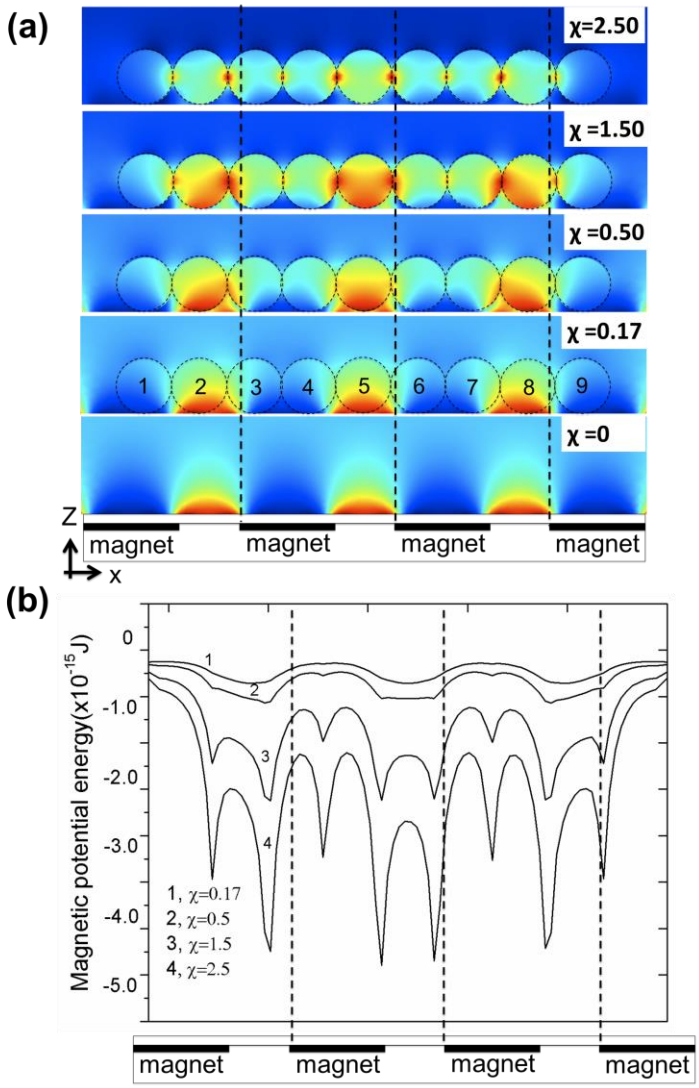

Fig. 7. Finite elements analysis of the magnetic potential energy distribution of an array of nine 2.8 micron diameter SPM beads on four 5 micron diameter micro-magnets (external magnetic field of 60 Gauss with θ_{xz}=0°). (a) Relative magnetic potential energy distribution of the chain of close-packed SPM beads (dashed circles) on the MMA with magnetic susceptibilities of 0, 0.17, 0.50, 1.5 and 2.5. The warm coloured areas represent areas of lower potential energy and thus attractive force. The attractive energies between beads occur at their point of contact and increases with increasing magnetic susceptibility. (b) Magnitude of the potential energy along the centre of the SPM beads as a function of *x*-position and susceptibility.